Development of a Surface Plasmon Resonance-Based Biosensing System

S. Mukherji, Munshi Imran Hossain, T. Kundu and Deepali Chandratre

Abstract Surface Plasmon Resonance (SPR)-based biosensing systems have become very popular among biologists and biochemists due to their ability to sense biomolecular interaction kinetics. It can be easily surmised that such systems may be of great use in diagnostic applications as well. However, the principal impediment to wide-scale deployment of these devices is the cost of the instrument. This effort to develop a low cost, widely deployable instrument was born out of a desire to initially popularize this instrument and technique among colleges and universities with budget constraints and move toward developing diagnostic applications on this platform. A low-cost device with significant sensitivity was developed, and this chapter describes the development on this front.

Keywords Surface plasmon resonance · Biosensor · Biomolecular interaction · Immobilization of antibodies · Optical detection

1 Introduction

This chapter discusses the development of a Surface Plasmon Resonance (SPR)-based biosensor. This is a kind of optical biosensor that makes use of SPR, a phenomenon that occurs due to the interaction of light with a metal–dielectric interface.

Biosensors may be defined as devices that use specific biochemical reactions mediated by isolated enzymes, immunosystems, tissues, organelles, or whole cells to detect chemical compounds usually by electrical, thermal, or optical signals [1]. Optical biosensing has some advantages over other sensing techniques. One

S. Mukherji (✉) · M. I. Hossain · T. Kundu · D. Chandratre
IIT Bombay, Mumbai, India
e-mail: mukherji@iitb.ac.in

important advantage of this class of sensors is that they are unaffected by electrical noise. This, in turn, makes the associated instrumentation system easy to design. Another advantage is that these sensors are easily given to microfabrication which allows for the possibility of miniaturization of the sensor and therefore smaller, portable instruments which can be used on fields.

Among the label-free, real-time optical biosensors, SPR is emerging as a very impactful phenomenon for making biosensors because of its high sensitivity and specificity.

1.1 Organization of the Chapter

The contents of this chapter can be broadly distinguished into the following parts that appear in order. The physics behind SPR, and how the phenomenon is exploited for biosensing, is explained. This is followed by a discussion of the setup that was used to perform experiments along with associated procedures. Thereafter, the results obtained have been discussed along with methods that were used to analyze the experimental data. The chapter concludes with a brief outline of the scope of future work in the development of this instrument.

2 Fundamentals of SPR and SPR-Based Sensing

The phenomenon of SPR occurs when light, more specifically *p*-polarized light, is incident on a metal–dielectric interface. At this interface, the light excites free electrons in the metal causing charge density oscillations. There are certain criteria that need to be fulfilled for the phenomenon to occur. These have been stated later in the chapter.

SPR was first reported by R. W. Wood in 1902 in his seminal paper [2]. When Wood allowed polarized light to be incident on a mirror with a diffraction grating on its surface, he observed a pattern of light and dark bands in the reflected light. The phenomenon was, however, explained later by Otto [3] and Kretschmann [4] independently in 1968. This phenomenon was first used for biosensing in 1983 by Liedberg et al. [5]. They used SPR for immunosensing and could detect the presence of a-IgG (anti-immunoglobulin G) down to 0.2 μg/ml.

When *p*-polarized (transverse magnetic) light passing through a prism is incident on a thin metal film, at an angle greater than the critical angle for the metal-prism interface, the light is reflected back due to total internal reflection. When the angle of incidence is changed, it is seen that the intensity of reflected light is at a minimum for a particular angle of incidence. At this angle of incidence, the light excites free electrons of the metal layer causing them to oscillate. This sets up oscillations in the charge density of the metal film. These charge density oscillations are known as plasmons. The field vector of this wave has maxima at the

interface of the metal and dielectric and decays exponentially into both the media
[6]. This is schematically shown in Fig. 1. The generated surface plasmon wave
(SPW) can travel up to a few microns along the surface.

The absorption of energy by the free electrons causes a reduction in the
intensity of the reflected light. The angle at which the intensity of reflected light is
minimum is the SPR angle.

In order to generate SPW, light that is polarized parallel to the plane of inci-
dence is required. Such a light ray is said to be TM (transverse magnetic) polar-
ized. The momentum vector k of TM polarized light may be resolved into two
orthogonal components, one of which is parallel to the metal surface. This com-
ponent of momentum, k_x excites plasmons at the metal–dielectric interface [2].

$$k_x = \left(\frac{\omega}{c}\right)\sqrt{\varepsilon}\sin\theta$$

In the equation, c is the speed of light in a vacuum, ω is the angular frequency
of light in a vacuum, and ε is the dielectric function of the coupling medium.

The necessary condition for the existence of the SPW is that the dielectric
constants of the two media, at whose interface the SPW is generated, are of
opposite signs. The real part of the permittivity for dielectrics is usually positive,
and that for metals is negative. In fact, metals such as gold, silver, and aluminum
have a negative real part of permittivity in the visible and near infrared region of
the spectrum [7]. The propagation constant, k_{sp} of the SPW is given by the fol-
lowing equation.

$$k_{sp} = \left(\frac{\omega}{c}\right)\sqrt{\frac{\varepsilon_M \varepsilon_D}{\varepsilon_M + \varepsilon_D}}$$

Here ε_M and ε_D are the dielectric functions of metal and dielectric, respectively.
The phenomenon of SPR occurs when

$$k_x = k_{sp}$$

For the phenomenon of SPR to occur, the real part of ε_M should be negative and
its absolute value must be smaller than ε_D. Metals like gold, silver, aluminum, etc.,
have a negative real part of permittivity in the visible and near infrared region of
the spectrum. A major field of the SPW is concentrated in the dielectric, so the
propagation constant of the SPW is sensitive to refractive index changes of the
dielectric [6].

Direct excitation of the metal–dielectric interface cannot cause SPR. Another
condition that should be satisfied is that the wave vector propagating along the
interface between metal and dielectric should be equal. The wave vector of light in
free space (k_o) is usually smaller than the wave vectors of surface plasmons
propagating along the interface (k_{sp}). This warrants a higher refractive index
material such as prisms, gratings, and optical waveguides that help to match the
propagation constant of the light wave to that of the SPW.

Fig. 1 Distribution of magnetic field intensity for a SPW at the interface between gold and dielectric (r.i. = 1.32) in the direction perpendicular to the interface, wavelength = 630 nm and 850 nm [21]
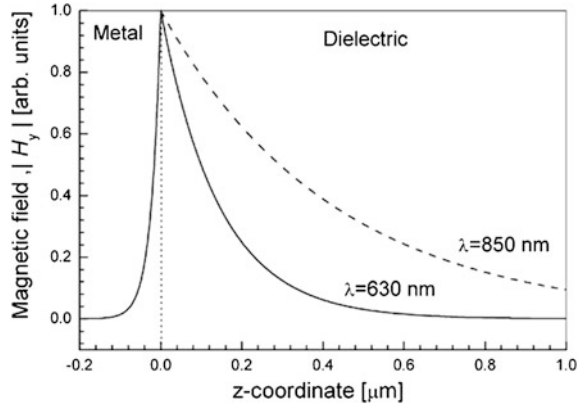
There are three main methods of coupling *p*-polarized light into the metal–dielectric interface. These are:

1. Prism-coupled system
2. Optical waveguide coupling-based system
3. Grating coupler-based system.

2.1 Prism-Coupled System

The most common configuration in which prisms are used is the Kretschmann configuration. A light wave is passed through a prism of a high refractive index and suffers total internal reflection from the base of the prism. The evanescent field thus generated penetrates through the thin metal layer at the base of the prism and excites plasmons in the metal film. By adjusting the angle of incidence of the light, the propagation constant of the evanescent wave can be matched with that of the SPW, i.e.,

$$\left(\frac{\omega}{c}\right)\sqrt{\varepsilon}\sin\theta = \text{Re}\{k_{\text{sp}}\}$$

This configuration is schematically shown in Fig. 2.

In this project, an SF11 (refractive index (r.i.) = 1.778) prism is used in the Kretschmann configuration. The prism is hemicylindrical in shape which ensures that the incident light is always normal to the curved surface of the prism and, hence, prevents refraction of the light at this face.

Fig. 2 Prism-coupled SPR configuration [6]
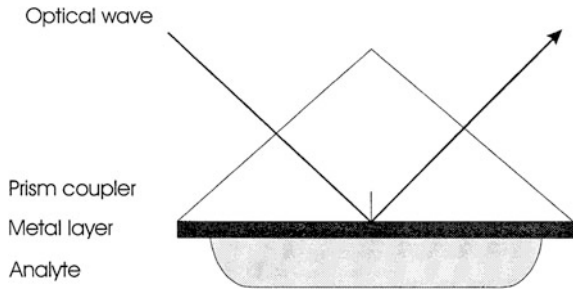
2.2 Optical Waveguide Coupling-Based System

Optical waveguides are structures that guide light waves. These are also called optical fibers. When light passes through an optical waveguide it generates an evanescent wave at the core–cladding interface. If a part of the fiber is decladded and coated with a metal film, surface plasmons can be excited in this region by the evanescent wave. The metal film can be suitably processed for biosensing applications. Figure 3 is a schematic of the optical waveguide coupling system.

2.3 Grating Coupler-Based System

Diffraction gratings are used to couple the light to the metal film. Sinusoidal gratings are used most often. The component of the wave vector of the diffracted waves parallel to the interface is diffraction-increased by an amount which is inversely proportional to the period of the grating and can be matched to that of an SPW [8]. This method of coupling is illustrated in Fig. 4.

Unlike in the other two configurations, in grating-coupled systems, the light passes through the sample solution resulting in a decreased signal from the sensor [8].

2.4 Metals for SPR: Their Thickness and Reflectance

For SPR, metals must have a band of electrons capable of resonating at a particular wavelength. The metals for SPR must have their resonating wavelength within the electromagnetic spectrum. They should also be highly pure for good resonance because the formation of oxide, sulfides, etc., on the metal surface can make performance of SPR deteriorate.

Metals that can be used for SPR are silver, gold, copper, aluminum, sodium, and indium. Indium is very expensive, sodium too reactive, copper and aluminum are too broad in their SPR response, and silver too susceptible to oxidation though it has a longer propagation length of SPW resulting in a very fine and sharp dip, as

Fig. 3 Optical waveguide being used to couple light to a metal layer [6]
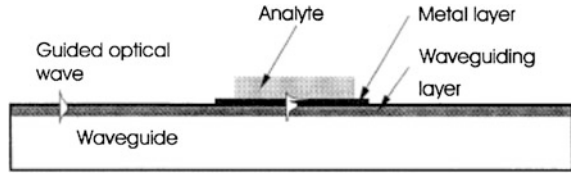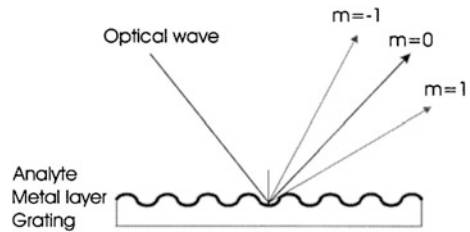

Fig. 4 Diffraction grating used for light coupling to a metal film [6]

shown in Fig. 5 [9]. Gold is very resistant to oxidation, and is compatible with many biochemical interactions, but has a shorter SPR propagation length resulting in a broad dip, as shown in Fig. 5. A silver–gold bimetallic layer is used, in which the silver sustains the SPW and the gold layer provides a biochemically stable surface. The total thickness of the metal layer is about 50 nm for proper resonance. The effect of different metals on the sharpness of the reflectance minimum is shown in Fig. 5.

The thickness of the metal films also affects the reflectance of light. The best contrast is obtained around 55 nm and it progressively deteriorates on both the higher and lower side, as shown in Fig. 6 [10]. The adhesion layer material like chromium, titanium, etc., and its thickness can also affect the contrast of dip.

2.5 SPR Used in Biosensing

The conditions for SPR are very sensitive to changes in the optical properties of the dielectric medium adjacent to the metal film. Therefore, changes in this dielectric medium can be monitored by the interaction of the SPW and the polarized light. A change in the refractive index of the dielectric on the metal film, changes its permittivity. This causes a change in the k_{sp} of the surface plasmon. As a result, the condition for resonance is satisfied for a different incident angle (if the wavelength is constant)—angular interrogation; or at a different wavelength (if the angle of incidence is constant)—wavelength interrogation.

SPR-based sensors are used for studying antigen-antibody binding, protein–protein, and protein–DNA (de-oxy ribonucleic acid) binding. In the biosensors, a biorecognition element is immobilized on the surface of the sensor. A binding reaction causes a change in the refractive index of the dielectric layer and, therefore, the condition for SPR. The change in the refractive index produced by

Fig. 5 Experimental SPR curves showing effect of metal on dip broadness with BK7prism and glucose solution [22]
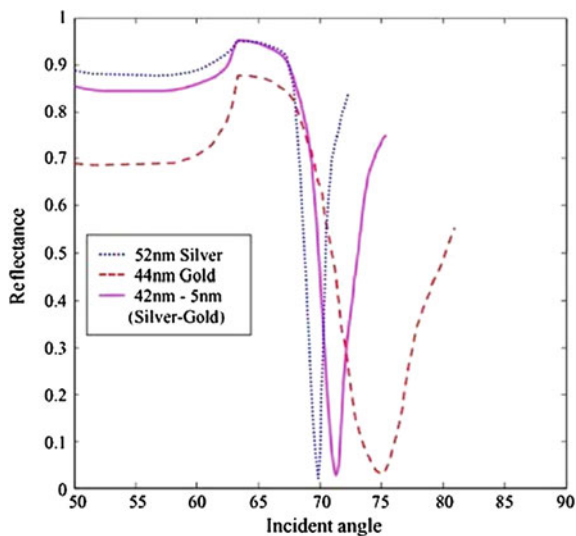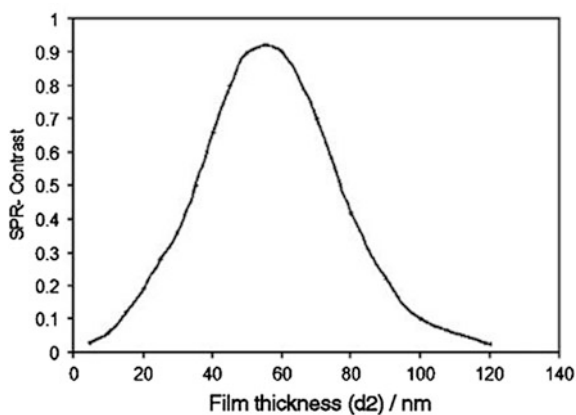
Fig. 6 SPR dip contrast versus metal thin film thickness [10]

the capture of analyte molecules depends on the concentration of the analyte molecules at the sensor surface. Figure 7 shows the schematic of the principle of biosensing in SPR.

3 The Experimental Setup for SPR

A substantial amount of work has been done on prism-based SPR biosensors at the Bioinstrumentation group, in IIT Bombay. Initial angular experiments were carried out using a He–Ne laser (632.8 nm), polarizer, focusing optics, rotary stage, and an
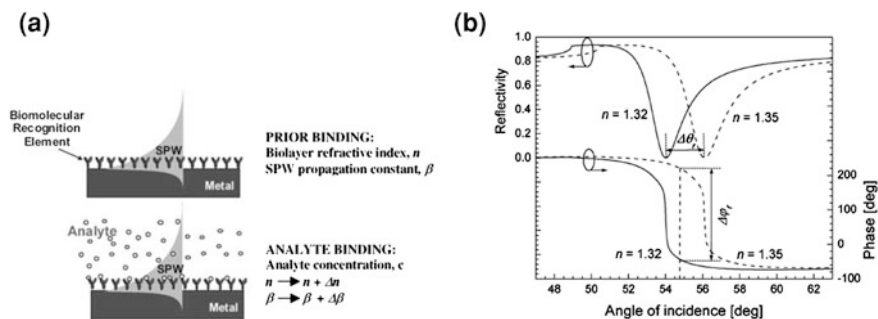
Fig. 7 a Schematic illustration of the concept of biosensing by SPR and **b** shift in reflectance minima because of change in dielectric medium [21]

optical power meter. Initial studies have reported characterization of the metal film thickness and the effect of different refractive indices on the dip characteristics [11, 12].

The metal layer was directly sputtered on the surface of the SF10 (r.i. = 1.728) triangular prism or BK7 (r.i. = 1.515) hemicylindrical prism. Later, BK7 coverslips were sputtered with the metal layer and coupled to the BK7 prism using index matching oil (r.i. = 1.513, Invitrogen, USA). The cysteamine-glutraldehyde protocol and MuA (11-Mercapto-undecanoic acid)-EDC (N-(3-Dimethylaminopropyl)-N' ethyl-carbodiimide hydrochloride)/NHS (N-Hydroxysuccimide) protocol for immobilizing antibodies were also experimented with [13, 14].

Figure 8 shows the angular interrogation setup that was initially used. It used a 512 pixel linear CMOS (complementary metal oxide semiconductor) detector (S9227, Hamamatsu Photonics, Japan) to detect the dip in reflected light. The detector has a pixel pitch of 12.5 microns and a height of 500 microns. A microcontroller MSP430-based circuit was used to control the CMOS detector, and was serially interfaced to PC [15]. A Lab windows CVI-based program was developed to display and store data.

This setup was subsequently modified. The source of light was changed to a red laser diode (635 nm) DL-3148-025(Sanyo, Japan). The laser diode has a vertical beam divergence of 30° on both sides of the lasing layer and a horizontal beam divergence of 10° on both sides of the lasing layer. This laser diode oscillates in the TM mode. The polarization direction is perpendicular to the junction plane. Thus, the light emitted by the laser diode contains *p*-polarized components. By properly orienting the laser diode, the need for a polarizer was eliminated. It is followed by a biconvex lens with a focal length of 50 mm and a diameter of 12.7 mm held in a plastic lens holder. The metal-sputtered coverslip coupled to the BK7 prism using index matching oil is placed on a rotary stage such that the metal side of the coverslip faces the Teflon flow cell. The flow cell has an inlet and outlet tubing. An analyte is inserted into the flow cell with the help of a syringe. The prism-flow cell holder is mounted on a rotary stage which, in turn, is mounted on a platform with railings for *x* and *y* translations. The *z*-axis translation was achieved

Fig. 8 Angular interrogation setup for SPR experiments [17]

using a support screw system. CMOS linear image sensor-S9227 was used to capture the SPR dip, the same one used in the previous setup.

In the horizontal setup mentioned above, the flow cell and the analyte in the flow cell remain vertical during the experiments. This position is mechanically unfavorable for liquid analytes. So, there was a need for a setup in which the flow cell remains horizontal and the setup remains portable. The setup was therefore modified to a vertical angular interrogation setup as shown in Fig. 9.

It consists of a modular prism holder and a flow cell. The prism with a metal-sputtered coverslip coupled to it was tightened on the prism holder such that the metal side of coverslip faced the Teflon flow cell. The laser diode and the biconvex lens were mounted on the railing-mounted rotary stage. With this type of arrangement, the focal point does not shift when the source is rotated. The holder for the 512 pixel CMOS detector array was a right-angled bracket on which the PCB (printed circuit board) for the detector was mounted. The detector had to be manually moved and positioned to detect the dip.

All the previous SPR angular interrogation setups were portable, but a need was felt to develop a small, light-weighted, rugged, user friendly, semi-automated, and modular setup. The new portable setup was designed to be used as a vertical or a horizontal setup, with motion of the source and detector in synchrony in opposite directions, to track light and the simple assembly and fabrication of modules. The setup is shown in Fig. 10 and is described below.

The framework and supports for various components such as—a beam restrictor, prism platform, and coverslip platform were all made of acrylic sheets. This drastically reduced the weight of the setup, and also the size, to an extent.

The detector PCB was mounted on the vertical acrylic sheet. A polarizer in the p-polarization direction was placed over the CMOS detector. The analog video signal from the detector was digitized with an internal analog to digital converter and was serially transmitted. A Lab Windows-based program was used to receive serially transmitted data from the microcontroller and display it. A regulated
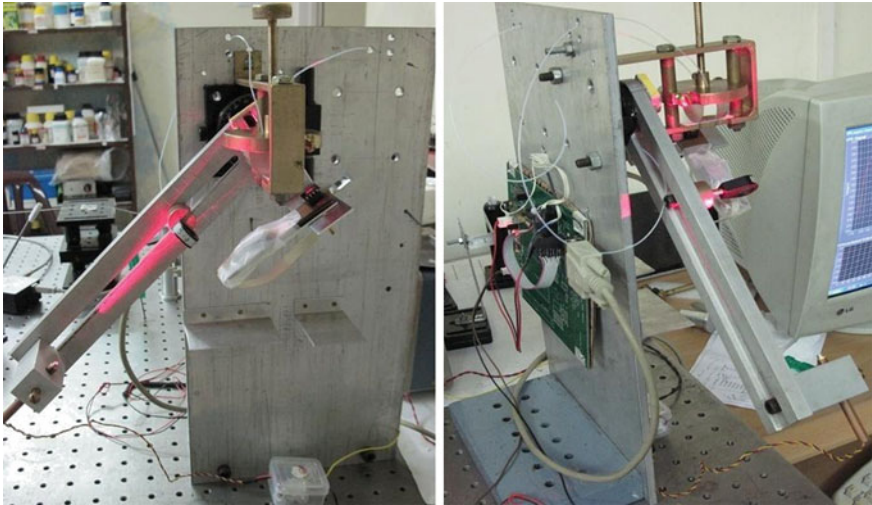
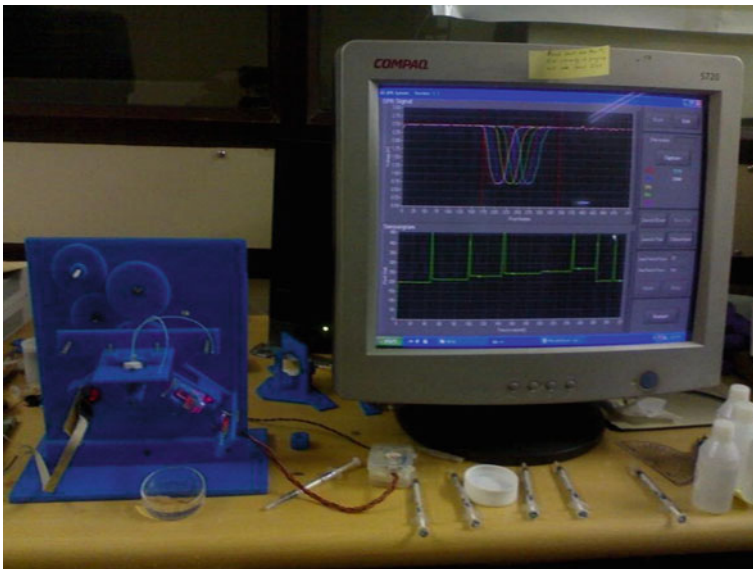**Fig. 9** Vertical angular interrogation setup for SPR experiments [17]

Fig. 10 Acrylic-based portable angular interrogation setup used in tests [16]

power supply (Tektronix PS280) was used to supply DC voltages to the MSP430 board and the laser diode driver.

However, it was not the kind that could be handheld and, hence, was not deployable in the field. This setup was subsequently modified to make it handheld and more modular than it was, previously. The electronics part of the instrument

was housed in a separate compartment, thereby isolating the areas (optical and fluidic) where there might be an ingress of water. The cover slip sputtered with metal, and the flow cell, are components that need to be frequently replaced in the system. Therefore, a provision was made for these in the upper exposed part of the instrument. The remaining part of the instrument below these has been covered, as shown in Fig. 11, and is not accessible to the user.

4 Experiments and Results Using Sucrose Solutions

The new setup was used for sucrose calibration tests. This required the preparation of the active sensor surface. This active surface is the metal-sputtered cover slip.

SF11 glass prisms (r.i. = 1.778) and cover slips (Lensel Optics, Pune) were used for the experiments. The cover slips were of size $18 \times 18 \times 0.5$ mm. The refractive index matching fluid (r.i. = 1.785, Cargille, USA) was used to couple the cover slip to the prism.

Sucrose solutions of different concentrations were used for the calibration of the sensor. The different concentrations of Sucrose GR (Merk Chemicals) were prepared in deionized water (r.i. = 1.33299). The different concentrations of sucrose were approximately 2 % (r.i. = 1.33587), 5 % (r.i. = 1.34026), 8 % (r.i. = 1.34477), 10 % (r.i. = 1.34783), and 12 % (r.i. = 1.35093) wt/wt.

4.1 Preparation of the Active Sensor Surface

The cover slip surface is sputtered with Ti–Au. However, before the sputtering, this surface needs to be cleaned appropriately so as to remove contaminants. The following procedure is followed to clean the cover slips [16].

4.1.1 Cleaning of Cover Slips

1. Sulfochromic acid cleaning: The cover slips, after antigen–antibody or sucrose calibration experiments, need to be recycled. The cover slips were kept in sulfochromic acid for 24 h which removes gold and other impurities from the surface. Later, these cover slips were rinsed in deionized water.
2. Etching of metal: Sometimes, sulfochromic acid is unable to remove gold and the metal layer beneath the gold sensing layer completely. Hence, a gold etching solution (potassium iodide and iodine) was used to etch the gold and followed by rinsing in concentrated HCl (to remove titanium).
3. Sonication in acetone: The cover slips were then immersed in acetone in a Petri dish and sonicated for 15 min. The cover slips were rinsed in deionized water and dried in a nitrogen jet.

Fig. 11 The portable SPR
setup [23]

4. Piranha cleaning: A Piranha solution is a mixture of 30 vol. % H_2O_2 and 70
   vol. % H_2SO_4. The Piranha solution, being highly reactive, removes organic
   and inorganic contaminants. Then, the cover slips were rinsed in deionized
   water and dried in a nitrogen jet.

4.1.2 Metal Sputtering

The cleaned SF11 cover slips were then sputtered with a bimetal layer in a metal
sputtering system (NORDIKO Metal Sputter) at Electrical Engineering, IIT
Bombay. The sputter chamber is vacuumised and then filled with Argon gas. The
metal to be deposited is the cathode and the cover slips (substrate) are the anode.
Argon plasma is used to deposit metals on the samples.

The sputtering time influences the thickness of metal deposition. Previous work
has optimized the sputtering time and temperature for the Ti–Au bilayer [17]. The
cover slips were first sputtered with titanium for 35 s at 150 W and gold for 50 s at
80 W.

4.2 Experimental Procedure

The cover slip is cleaned with isopropyl alcohol prior to use. A drop of index matching fluid is introduced on the flat surface of the prism, and the metal-sputtered cover slip is placed on the prism with the metal side facing out. The flow cell is then placed on the cover slip and tightened with the help of acrylic pieces on the sides of the module using nuts.

The laser is powered on, and the arm on which it is supported is rotated to obtain a dip in the reflection spectra. The spectrum is viewed on a computer with the help of a DAQ (data acquisition) card and software developed for this system. An appropriate filter is chosen to get a smooth output. The dip with air as dielectric is obtained at around 37°.

Using a syringe, analytes (different concentrations of sucrose solutions in water) are injected into the flow cell. The source arm is moved to appropriate angles to obtain a dip. By setting the proper pixel limits for finding the minima, a sensor-gram is started so as to track the minima with respect to time. During the SPR experiments, a background reading is established in deionized water. With deionized water set as the background, a series of sucrose solutions are injected into the flow cell and recorded using a CMOS detector.

When deionized water is injected back after a 12 % sucrose solution, the minima is found to revert back to nearly the same pixels as at the beginning of the experiment.

A refractive index change from deionized water (r.i. = 1.33299) to 12 % sucrose (r.i. = 1.35093) was used for sensitivity calculations. The minima shifted by 74 pixels giving a sensitivity of 0.242 mRIU/pixel.

The results of the sensor calibration experiments using different concentrations of the sucrose solution are shown below in Figs. 12 and 13.

4.3 Data Analysis

An algorithm is implemented with the aim of finding the pixel at which resonance occurs which can consequently give a measure of the SPR angle and, therefore, the r.i. of the analyte. The algorithm was proposed by Thirstrup and Zong [18]. The algorithm essentially finds the centroid of the SPR profile. However, it uses a dynamic baseline that can compensate for fluctuations in the intensity of the light source and any dark signal from the detector. A diagrammatic representation of the concept is shown in Fig. 14. The algorithm is described in the following steps:

1. A dynamic baseline P_B is chosen according to the following equation [18],

$$\gamma A_0 = \gamma \int_{\theta_0}^{\theta_1} (P_B - P(\theta))d\theta = A_1 = \int_{\theta_1}^{\theta_2} (P_B - P(\theta))d\theta$$
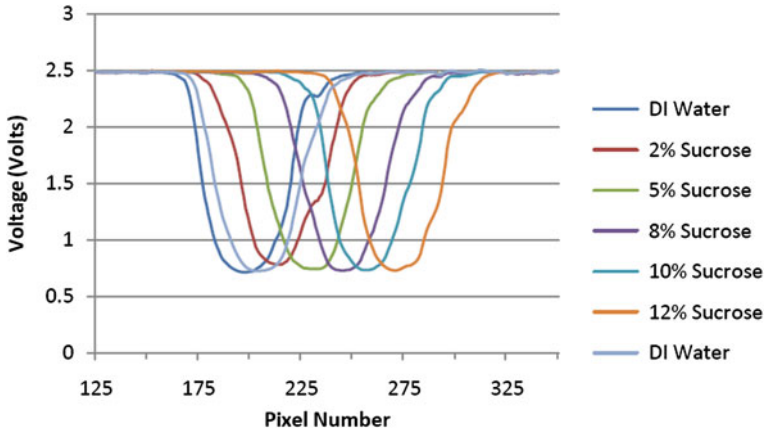
Fig. 12 Results of sensor calibration using sucrose on Ti–Au cover slip that is continuously heated at 125 °C by sputtering
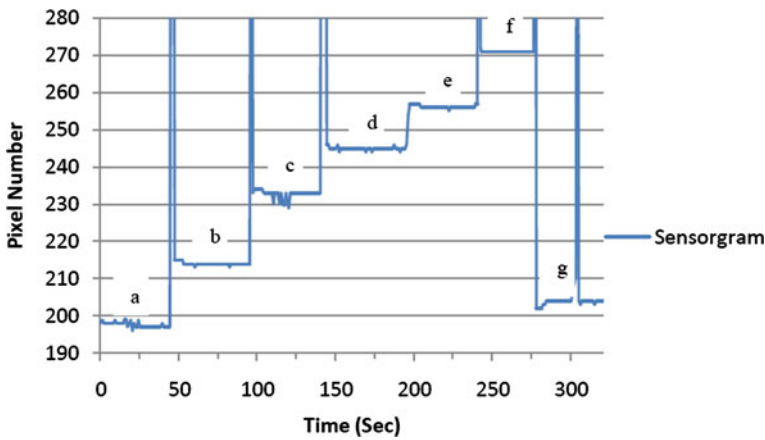

Fig. 13 Sensorgram for the sensor calibration experiment with Ti–Au-sputtered cover slip continuously heated at 125 °C (detector distance: 50 mm). (*a, b, c, d, e, f,* and *g* are minima positions when deionized water, 2, 5, 8, 10, 12 % sucrose solutions and deionized water are injected, respectively)

In the discrete domain, this equation may be written as,

$$\gamma\left(\sum_{\theta=\theta_0}^{\theta_1} P_B - P(\theta)(\theta_1 - \theta_0)\right) = \left(\sum_{\theta=\theta_1}^{\theta_2} P_B - P(\theta)\right)(\theta_2 - \theta_1)$$

The criterion for choosing γ is that there should be a sufficient number of data points in A_0 and A_1.

Fig. 14 SPR profile with the dynamic baseline P_B and the areas A_0 and A_1 of the curve *above* and *below* it, respectively [18]
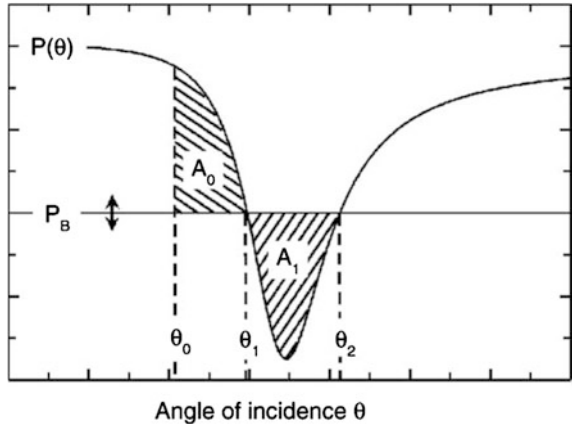
Therefore, $P_B = \dfrac{\gamma \sum\limits_{p=p_0}^{p_1} P(p) - \sum\limits_{p=p_1}^{p_2} P(p)}{\gamma(p_1-p_0+1)-(p_2-p_1+1)}$ where p is the pixel number.

2. The algorithm suggested in [18] uses an SPR profile that is plotted against the angle of incidence. However, this may also be implemented using an SPR profile that is plotted against a pixel number, since the pixel number has a one-to-one correspondence with the angle of incidence. Accordingly, the equation that is used to compute the centroid is,

$$\text{Pixel}_{\text{resonance}} = \frac{\sum\limits_{i=i_1}^{i_2} \left(P_{i,b} - P_i\right)i}{\sum\limits_{i=i_1}^{i_2} \left(P_{i,b} - P_i\right)}$$

3. The centroid may be taken as a reasonable estimate of the pixel at which resonance occurs. The SPR angle may be estimated by a linear transformation from the pixel number domain to the angle of incidence domain.

The centroid calculation from the raw data, however, is not very reliable. This is because the noise in the photo detector and source intensity fluctuations can affect the output of the algorithm. In order to overcome this shortcoming, a local similarity matching algorithm is used on the raw data.

This algorithm [19] computes a moving dot product on the SPR profiles obtained for air and liquid (analyte in solution). The regions where the profiles are very similar give a high value for the dot product and a low value (valleys in the curve) for regions where the greatest dissimilarity occurs. The position of the valleys is where the resonance occurs. This algorithm is robust in the sense that it is better immune to noise in the data. The centroid algorithm can now be applied to this data to obtain an estimate of the minima. The governing equation for this algorithm is,

$$\cos \theta_{j,s} = \frac{L_{j,s}A_{j,s}}{|L_{j,s}||A_{j,s}|} = \frac{\displaystyle\sum_{i=j-s/2}^{j+s/2} l_i a_i}{\sqrt{\displaystyle\sum_{i=j-s/2}^{j+s/2} l_i^2 \sum_{i=j-s/2}^{j+s/2} a_i^2}}$$

where L and A are vectors of lengths of elements l and a, respectively, from SPR profiles of analyte and air, respectively.

The following curves, shown in Fig. 15, were obtained for the air and liquid (analyte in solution).

The voltage levels at each pixel comprise elements of a vector, one each for air and analyte. These vectors are used for the computation of a moving dot product.

The values of $\cos \theta$ so obtained can be interpreted as follows: In regions where the value is close to 1, the profiles are nearly similar. At places, where there is a wide disparity in the profiles, the value of $\cos \theta$ is low. At these positions, valleys are seen to occur. The SPR angle for air is usually higher than that for analytes. Therefore, valleys at the lower end are indicative of resonance due to analytes. These can now be inspected using a dynamic baseline centroid algorithm to obtain an estimate of the pixel at which resonance occurs.

The local similarity matching gives multiple valleys in the $\cos \theta$ profile. This makes it difficult to choose the correct valley to estimate the minima.

The dynamic baseline algorithm was then implemented using the SPR profiles that were obtained from the experiments. The output of the algorithm is an estimate of the pixel number at which resonance occurs. This is, then, transformed into the angle domain using the following equation.

$$\theta = \left[\left(9.642 \times 10^{-3} \right) \times p \right] + 46.893$$

This equation is obtained by a linear transformation using the pixels at which resonance occurs and the standard SPR angles for the sucrose solutions. This equation is, however, specific to the 512 pixel linear CMOS detector and the SF 11 prism used in the system. The estimated r.i. is then calculated using the following equation [18]

$$n_s = n_p \times \sin\theta$$

where n_s is the r.i. of the analyte and n_p is the r.i. of the SF 11 prism (=1.778).

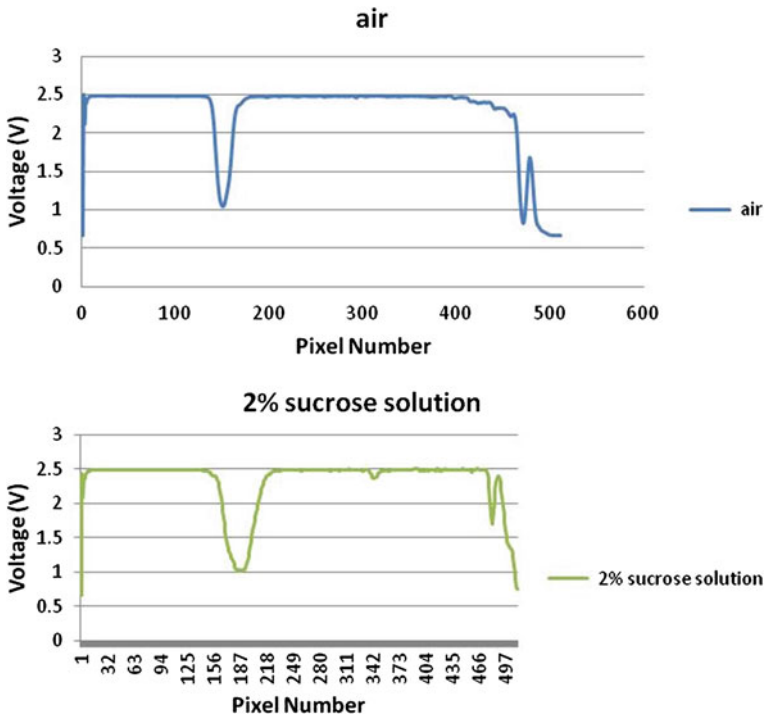The results are depicted in the graph shown in Fig. 16.

Fig. 15 SPR profiles obtained for air and 2 % sucrose solution

5 The SPR System in Biosensing

The primary purpose of an SPR system is to assess the kinetics of biomolecular interactions using the SPR phenomenon. The tests using sucrose solutions of varying concentrations revealed that the system is capable of resolving refractive index variations in the microenvironment of the metal surface down to a few milli-RIU (refractive index units) or even micro-RIU. In order to use the system for biosensing, the metal layer had to be modified for immobilization of biological receptor molecules on the surface. The most common forms of biorecognition events used in biosensing are:

(1) Antibody–antigen interactions,
(2) Nucleic acid interactions,
(3) Enzymatic interactions,
(4) Cellular interactions (i.e., microorganisms, proteins), and
(5) Interactions using biomimetic materials (i.e., synthetic bioreceptors).
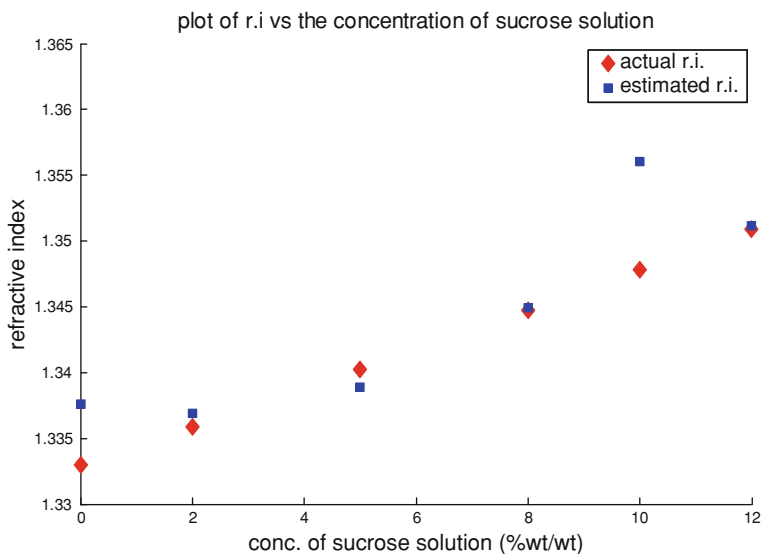
Fig. 16 Plot showing the actual and the estimated r.i. values versus the concentration of sucrose solution. The Euclidean distance or 2-norm error was calculated for the obtained estimates. This is equal to 0.0096. This figure suggests that most of the estimated values are within an error margin of 1 %

5.1 Immobilization of Antibodies

In our experiment, we used antigen–antibody interactions as biological recognition events that could be sensed using the SPR system. In this case, the antibodies were immobilized on the gold surface. For covalently binding antibodies on gold, two types of approaches were used.

5.1.1 Cystamine–Glutaraldehyde

- **Preparation of Buffer**: (PBS) Phosphate buffer saline (Ph: 7.4; 10 mM) was made by dissolving a PBS buffer tablet in 1000 ml water.
- **Cleaning of gold surface**: Coverslips coated with gold were first soaked in a 1.2 M NaOH solution for 5 min, then washed in DI (deionized) water followed by incubation in 1.2 M HCl for 5 mins, and again washed with DI water.
- **Cystamine layer on substrate**: The surface was incubated in cystamine solution (10 mM cystamine in 50 mM PBS, Ph: 7.4) for 1 h at room temperature. The surface was then washed with a buffer 2 or 3 times and dried using a nitrogen air jet.
- **Glutaraldehyde binding**: 10 % of Glutaraldehyde was added and incubated for 30 min. The surface was washed 2 or 3 times with a buffer. The surface was then ready for immobilizing antibodies.

- **Antibody immobilization**: Substrates were incubated in a 0.02 mg/ml of Goat anti-Human IgG antibody solution prepared in phosphate buffer saline (PBS pH 7.4). After an overnight incubation at 4 °C, the substrates were washed in PBS thoroughly to remove any loosely adsorbed molecules.
- **Antigen detection**: The immobilization of antibodies on the surface was tested by subjecting the surface to different concentrations of FITC (Fluorescein isothiocyanate)-tagged Human IgG antibodies for 10 min.

5.1.2 MuA: EDC–NHS Protocol

- **Cleaning of gold surface**: Coverslips coated with gold were first soaked in a 1.2 M NaOH solution for 5 min then washed in DI water followed by incubation in 1.2 M HCl for 5 min and again washed with DI water.
- **MuA layer on substrate**: The surface was incubated in a MuA solution (0.1 M MuA in absolute ethanol) for 30 min at room temperature. The surface was then washed with absolute ethanol 2 or 3 times followed by DI water and dried using a nitrogen air jet.
- **EDC–NHS Crosslinking**: The MuA-coated coverslips were then incubated in a solution of NHS (60 mM in DI water) and EDC (30 mM in DI water) for 2 h. Following this, the surface was washed 2 or 3 times with DI water making it ready for immobilizing antibodies.

Antibody preparation: Substrates were incubated in a 0.02 mg/ml of Goat anti-Human IgG antibody solution prepared in phosphate buffer saline (PBS pH 7.4). After an incubation of 40 min at room temperature, substrates were washed in PBS thoroughly to remove any loosely ordered molecules. The rest of the procedure is the same as earlier (Fig. 17).

5.2 Antigen–Antibody Interactions

5.2.1 Detection Using Cystamine Protocol

A BK7 prism was coupled with a coverslip sputtered with a silver–gold bilayer. An antibody (Goat anti-human IgG—GaHIgG) was immobilized on the metal bilayer using cystamine protocol. The SPR response was recorded after completion of the whole treatment of immobilizing with water as dielectric. This set of reading acts as a reference. Following this various concentrations of Human IgG antibodies were injected into the flow cell and the results were captured (Fig. 18).

From the graph (Fig. 19) and table (Table 1), we can see that there is minimum variation at the tip, whereas the variation was highest at two-thirds of the first half of the slope (15.6 mV/1 nM) and second highest at the middle of the second half of slope (8.7 mV/1 nM). In MSP430, a 12-bit ADC (analog to digital converter)

BK7 Coverslip

↓

50 nm Silver-Gold bilayer sputter

↓

Cleaning of Gold Surface

SAM layer of MuA   SAM layer of Cystamine

↓   ↓

EDC-NHS cross linker   Glutaraldehyde

↓   ↓

GaHIgG antibodies   GaHIgG antibodies

Fig. 17 Flow diagram summarizing the sample preparation procedure
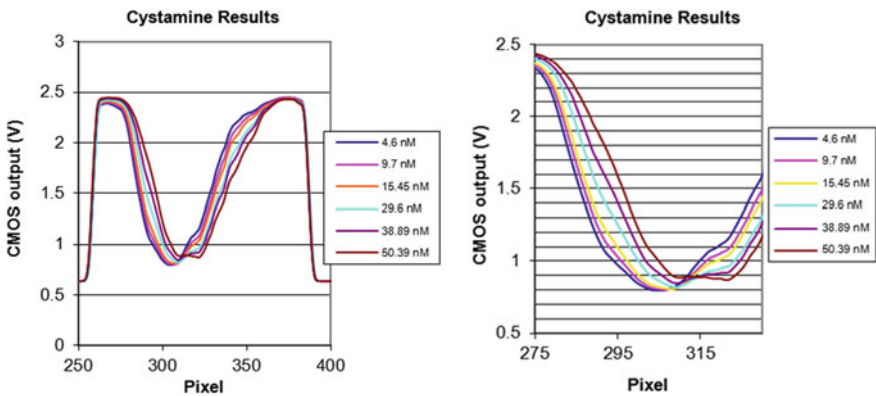
Cystamine Results

Cystamine Results

Fig. 18 Output on CMOS detector array using varying concentrations of HIgG antibodies as analytes after immobilizing GaHIgG antibodies using cystamine protocol to test for immobilization

(2.5 V full range) is used. Thus, we have 2.5 V distributed over 4096 bits. This leaves us with a resolution of 0.6 mV/bit. Even if we allow noise within 5 bits, we have a resolution of 3 mV/5 bits.

The first half of the slope is steeper than the second half of the slope. This also means that a span of analog data represented by one pixel is greater in the case of the first half slope than in the second half slope. Therefore, we can observe that despite having a better deflection on the first slope, the results are more clubbed together as compared to the second half. In the second half slope, the difference due to changing concentrations can be easily made out. Thus, it can be said that
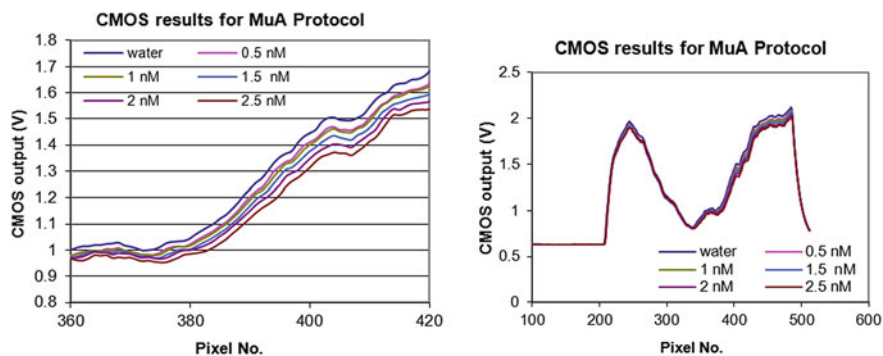
Fig. 19 CMOS sensor output for varying concentrations of HIgG antibodies in water for GaHIgG antibodies immobilized using MuA–EDC–NHS on silver–gold bilayer

Table 1 Comparison between concentration and reflectivity at various pixel positions for cystamine-coated slides

Concentration	Concentration	CMOS output (V)			
Nm	(ug/ml)	Pixel: 306 (tip)	Pixel: 291	Pixel: 345	Pixel: 328
4.6	0.66	0.797	1.063	2.232	1.538
9.7	1.393	0.805	1.135	2.177	1.446
15.45	2.218	0.819	1.219	2.116	1.376
29.6	4.26	0.863	1.400	2.003	1.253
38.89	5.58	0.916	1.584	1.945	1.207
50.39	7.23	0.998	1.788	1.820	1.115
Slope		**0.004**	**0.0156**	**−0.0086**	**−0.0087**

calculations on the second half slope would give the optimum bargain between resolution constraints due to ADC and sensitivity of detection.

Another important thing that should be noticed in the graph is that all 512 pixels do not participate in detection. Only that part of the CMOS sensor on which the laser output falls is analyzed, and is of interest. As we increase the distance between the reflecting surface and the sensor, the intensity of light decreases and the width of the dip broadens. Thus, if we place the sensor at an optimum position such that the laser output has sufficient measurable intensity, the dip would get broadened up. This would reduce the span of the analog data represented by one pixel which would, in turn, increase sensitivity.

5.2.2 Detection Using MuA–EDC–NHS Protocol

This prism had a refractive index of 1.515. In this case, first silver was sputtered for 20 s and then gold for 20 s, on a BK7 coverslip which was later coupled with the prism using an index matching fluid. Antibodies (Goat anti-human IgG

Table 2 Comparison between concentration and reflectivity at various pixel positions for MuA–EDC–NHS-coated slides

Concentration (nM)	Pixel No 390	Pixel No 400
0	1.232	1.445
0.5	1.202	1.411
1	1.191	1.400
1.5	1.169	1.376
2	1.1503	1.347
2.5	1.121	1.314
Slope	**−0.04192**	**−0.04978**

antibody) were immobilized on the metal bilayer by MuA SAMs (self-assembled monolayers) activation and EDC–NHS crosslinking. After completion of the whole treatment of immobilizing, the SPR response was recorded with water as dielectric, and at varying concentrations of Human IgG antibodies. The CMOS sensor output for varying concentrations of antibodies and water was seen as in Fig. 19. It is possible that the relationship between the resonating angle and refractive index is Gaussian. However, in this narrow range, it was found to be close to linear.

As can be seen, 73 ng (i.e., 500 pM) of antibodies were injected into the flow cell and were successfully detected. Table 2 shows that the sensitivity of the system was approximately 50 mV for 1 nM. Thus, comparing with ADC resolution and noise constraints, the minimum concentration that could be detected would be about 60 pM.

6 Conclusions

The setup that is used currently is reasonably light in weight, modular, and portable. However, there are some directions in which more development may be done.

Other methods may be explored to improve the results that are obtained. These may involve suitable modeling of the system as a function of various parameters of interest such as the r.i. of the analyte, thickness of the analyte layer, etc.

The data analysis algorithms have been implemented in MATLAB. However, these can be easily converted to the C language and written into the MSP430 microcontroller that is used in the system. This will, then, make the system capable of being a standalone system without the need for an external computer for data analysis.

More work may be done to improve the mechanical design to make the setup user friendly. The feasibility of using Ag films may be explored as suggested in [20] because Ag films give a sharper dip in the SPR profile than Au films.

References

1. IUPAC (1997) Compendium of chemical terminology. In: McNaught AD, Wilkinson A (eds) The "Gold Book", 2nd edn. Blackwell Scientific Publications, Oxford (1997)
2. Wood RW (1902) On a remarkable case of uneven distribution of light in a diffraction grating spectrum. Philos Mag 4:396–402
3. Otto A (1968) Excitation of non radiative surface plasma waves in silver by the method of frustrated total reflection. Z Phys 216:398–410
4. Kretschmann E, Raether H (1968) Radiative decay of non radiative surface plasmons excited by light. Z Naturforsch 23:2135–2136
5. Liedberg B, Nylander C, LunDstrOm L (1983) Surface plasmon resonance for gas detection and biosensing. Sens Actuators 4:299–304
6. Homola J, Yee SS, Gauglitz G (1999) Surface plasmon resonance sensors: review. Sens Actuators B 54:3–15
7. Wolfbeis OS (2006) Springer series on chemical sensors and biosensors—methods and applications. Springer, Berlin
8. Homola J (1997) On the sensitivity of surface plasmon resonance sensors with spectral interrogation. Sens Actuators B 41:207–211
9. SPR pages (2011) Website http://www.sprpages.nl/SprTheory/SprTheory.htm. Accessed 15 May 2011
10. Neff H, Zong W, Lima AMN, Borre M, Holzhuter G (2006) Optical properties and instrumental performance of thin gold films near the surface plasmon resonance. Thin Solid Films 496:688–697
11. Dhananjay VP (2006) Surface plasmon resonance based biosensor for detection of waterborne pathogens. Master's thesis, IIT Bombay
12. Bharadwaj R (2007) Surface plasmon resonance based biosensor for detection of waterborne pathogens. Master's thesis, IIT Bombay
13. Chandratre D (2008) Development of a surface plasmon resonance based biosensor. Master's thesis, IIT Bombay
14. Tanneru K (2009) Design and development of hemi cylindrical prism based surface plasmon resonance biosensor. Master's thesis, IIT Bombay
15. Dhawangle A (2009) MSP430 applications in biomedical system. Master's thesis, IIT Bombay
16. Mhatre AK (2011) Development of a portable surface plasmon resonance system. Master's thesis, IIT Bombay
17. Monteiro J (2010) Development of a portable surface plasmon resonance biosensor. Master's thesis, IIT Bombay
18. Thirstrup C, Zong W (2005) Data Analysis for surface plasmon resonance sensors using dynamic baseline algorithm. Sens Actuators B 106:796–802
19. Owega S, Poitras D (2007) Local similarity matching algorithm for determining SPR angle in surface plasmon resonance sensors. Sens Actuators B 123:35–41
20. Abdelghani A et al (1997) Surface plasmon resonance fibre-optic sensor for gas detection. Sens Actuators B 38–39:407–410
21. Homola J (2003) Present and future of surface plasmon resonance biosensors. Anal Bioanal Chem 377:528–539

22. Ong BH, Yuan X, Tjin SC, Zhang J, Ng HM (2006) Optimised film thickness for maximum evanescent field enhancement of a bimetallic film surface plasmon resonance biosensor. Sens Actuators B 114:1028–1034
23. Hossain MI (2012) Development of a surface plasmon resonance based biosensing system. Master's thesis, IIT Bombay